Dynamics of Yb2+ to Yb3+ ion valence transformations in Yb:YAG ceramics used for high-power lasers

Dynamics of Yb^{2+} to Yb^{3+} ion valence transformations in Yb:YAG ceramics used for high-power lasers

Mykhailo Chaika[a,b], Oleh Vovk[b], Giulia Mancardi[c], Robert Tomala[a], Wiesław Strek[a].

[a]*Institute of Low Temperature and Structure Research Polish Academy of Science, ul. Okolna 2, 50-422 Wrocaw, Poland.*

[b]*Institute for Single Crystals, National Academy of Sciences of Ukraine, 60, Lenin Avenue, Kharkiv, 61001, Ukraine.*

[C]*Department of Chemistry, University College London, 20 Gordon St, London, WC1H 0AJ, UK.*

Abstract

Due to the good thermal-mechanical and luminescence properties, Yb:YAG ceramics are suitable as thin-disk lasers; however, their efficiency is limited by the presence of Yb^{2+} ions, which entail parasitic energy transfer from Yb^{3+} to Yb^{2+}. This article focuses on the Yb^{2+} formation in Yb:YAG ceramics prepared by solid-state reaction sintering. The samples were prepared by air annealing, the oxidation of the material leads to recharging Yb^{2+} ion to its trivalent state. The activation energy was determined by Jander to be $E_a(D) = 2.7\pm0.2$ eV, which is in good agreement with the activation energy for oxygen diffusion in the YAG lattice. It was concluded that the recharging of Yb^{2+} ion to its trivalent state in YAG ceramics is limited by the oxygen self-diffusion through the grain volume, and the oxygen vacancy alone and/or together with the presence of antisites can be proposed as Yb^{2+} charge compensation mechanism in the YAG ceramics, unlike the YbAG single crystals, where tetravalent impurities are responsible for charge compensation.

Keywords: optical ceramics, Yb:YAG, oxidation kinetics.

1. Introduction

Due to the good thermal and mechanical properties of the YAG ceramics and the advantages of using Yb^{3+} ions, namely (i) a small quantum defect between the pump and the laser photons, (ii) broad absorption bands and (iii) long fluorescence lifetime of the upper laser level, Yb^{3+}-doped YAG are

suitable for commercial high-power lasers, moreover, the possibility to incorporate ytterbium in a very high concentration, up to 100 at.% ($Yb_3Al_5O_{12}$), is especially advantageous for producing thin-disk lasers [1, 2, 3, 4]. Yb^{3+} doped YAG materials can be prepared by melt growth technique [5] as well as solid-state reaction sintering, [3, 6] obtaining single crystals and ceramics respectively. Transparent ceramics become more and more important for applications in which materials need to have good optical properties and resistance to extremely high mechanical and thermal stress [7, 8]. However, the 10 at.% Yb:YAG ceramic laser performance is worse than its counterpart single crystal, whereas the 20 at.% Yb:YAG ceramic is better [9].

One of the reasons of such behaviour might reside in the energy loss processes where the energy transfer of the Yb^{3+}-Yb^{2+} pair is followed by anti-Stokes white emission of Yb^{2+}-Yb^{3+}-ions pair, as evidenced by some authors [1, 10]. This phenomenon, commonly considered as a parasitic process in laser materials, originates from the intervalence charge transfer in the Yb^{3+}-Yb^{2+} pairs in the YAG matrix [11] and indicates that Yb^{2+} ions play a key role in the energy loss process. Yb-doped YAG ceramics originally include Yb atoms in its trivalent state, which can replace Y^{3+} ions. The formation of Yb^{2+} and the energy transfer in Yb^{3+}-Yb^{2+} pairs can take place during infrared laser excitation. The extra charge generated in the YAG lattice due to the Yb reduction should be compensated [12, 13]. The possible charge compensation mechanisms are the creation of oxygen vacancies, oxygen vacancies with antisites, displacement of the cation to an interstitial site and self-compensation [13].

The formation of Yb^{2+} ions is an important part of the energy loss process due to the energy transfer in the Yb^{3+}-Yb^{2+} pairs, therefore, understanding the nature of Yb^{2+} charge compensation mechanism would allow decreasing the occurrence of this parasitic process in laser materials. To our knowledge, few works related to the Yb^{2+}-Yb^{3+} ions valence transformation process have been published [14, 15], and a detailed mechanism of Yb^{2+} ions charge compensation has not yet been proposed due to the lack of supporting information.

The purpose of this study is to examine the Yb^{2+} charge compensation mechanism in the Yb:YAG ceramics as well as to propose a model for describing this process.

2. Experimental

$Yb_{0.3}Y_{2.7}Al_5O_{12}$ ceramics were synthesized according to the protocol described in our previous works [16, 17, 18] by reactive sintering using the high purity powders of Al_2O_3 (>99.99%, Baikowski, France; d ≈ 0.15–0.3 μm), Y_2O_3 (99.999%, Alfa Aesar; d ≈ 3-5 μm), and Yb_2O_3 (>99.99%, Alfa Aesar; d ≈ 5-10 μm). Tetraethylorthosilicate (TEOS) and zirconia ZrO_2 (≥99.99%, Alfa Aesar) in amount of 0.5 wt% (0.14 wt% SiO_2) were applied as a sintering aids. Powders were mixed according to YAG stoichiometry with 10 at% Yb replacing corresponding amount of yttrium. The obtained mixtures were ball-milled with ethanol alcohol in polyamide jar with ZrO_2 balls for 15 h using Pulverisette 5/4 (Fritsch GmbH, Germany) planetary ball mill underthe rotation speed of 140 rpm. Oven air-drying of the slurry for 1 day was followed by sifting through a 200-mesh screen. The powders were compacted by uniaxial pressing at P=250 MPa resultedg in pellets and followed annealed in air at 800 °C was applied to eliminate organic impurities. The Yb:YAG ceramics were obtained by sintering these pellets in a vacuum furnace with tungsten heating elements at 1750 °C under vacuum (6×10^{-3} Pa) for 10 h.

First, the pellets were polished to optical grade and, afterwards, they were annealed at different temperatures to study the oxidation kinetics by means of optical spectroscopy. For the optical investigation, the ceramics were stepwise polished by diamond slurries with a gradual decrease in the size of the abrasive from 30 to 7 microns. The resulting samples had an 8 mm diameter and a thickness of 1.2 mm. The ceramics were characterized by XRD spectroscopy, scanning electron microscopy (SEM) (JEOL JSM-6390LV) and absorption optical spectroscopy (Perkin Elmer Lambda 35). The oxidation of the ceramics was carried out in a special vacuum furnace with the capability to change the residual pressure in the chamber in a short time from the ambient pressure down to 4 Pa.

We performed a study of the oxidative kinetics of Yb ions at three different temperatures of 860, 890 and 920°C. Such temperature range was taken to compare the results of this work with those in literature [14,15]. The experiments were carried out following the steps: (I) loading of the sample into the vacuum chamber, which was evacuated to a pressure lower than 4 Pa; (II) heating of the chamber up to the selected temperature; (III) opening of the chamber to obtain a rapid rise in pressure which allows Yb^{2+} ions oxidation; (IV) evacuation of the furnace camera after a specific time; (V) cooling at

room temperature; these preparation steps were followed by the collection of the absorption spectra. To obtain the subsequent point on the kinetic curve, the samples were further oxidized at the same temperature for longer according to steps (I-V).

3. Results

The present investigation aims at unravelling the Yb^{2+} to Yb^{3+} ion valence transformation mechanism (further called Yb^{2+} oxidation) through the analysis of the variation of Yb^{2+} concentration in time during air annealing at three different temperatures in Yb:YAG ceramics prepared by solid-state reaction (SSR) sintering in a vacuum. In the next few paragraphs, we are going to present an overview of the existing knowledge on Yb^{2+} oxidation.

Originally, Yb incorporates into YAG lattice in its trivalent state. Vacuum sintering of the Yb:YAG ceramics should be considered as a heating process taking place in a reducing environment which causes the formation of Yb^{2+} ions [3]. During sintering, the oxygen in the crystal lattice evaporates as molecular species O_2, thus originating an oxygen vacancy and two electrons. Yb^{2+} ions formation can be schematically described by the following equations:

$$\ll YAG \gg \rightarrow V_O^{\bullet\bullet} + 2e' + {}^1\!/_2\, O_2 \uparrow \quad (1)$$

The electrons are trapped by the oxygen vacancy, generating F^+ colour centre (Eq. 2) or reducing Yb^{3+} ion to the divalent state (Eq. 3) [19]

$$V_O^{\bullet\bullet} + e' \rightarrow V_O^{\bullet} \quad (2)$$

$$Yb_Y^{*} + e' \rightarrow Yb_Y' \quad (3)$$

As a result, after vacuum sintering, Yb:YAG ceramics contain both Yb^{3+} and Yb^{2+} ions. Due to the process in reaction (Eq. 3), the number of electrons is not enough to reduce all the oxygen vacancies $V_O^{\bullet\bullet}$, so, a fraction of them remains in the lattice. Therefore, the following kinds of defects presumably exist in the crystal after vacuum sintering: oxygen vacancies $V_O^{\bullet\bullet}$, divalent Yb impurities and charged oxygen vacancies as colour centres $V_O^{\bullet}$.

Divalent impurities migrate near oxygen vacancies forming neutral aggregates in the garnet crystal lattice (Eq. 4) [20]

$$Yb'_Y + V_O^{\bullet} \rightarrow [Yb'_Y \ldots V_O^{\bullet}] \text{ (4)}$$

where $\ll YAG \gg$ - pure crystal, $V_O^{\bullet\bullet}$ - oxygen vacancy, $V_O^{\bullet}$- F^+ colour centre, Yb_Y^* - Yb^{3+}, Yb'_Y - Yb^{2+}.

Air annealing can be applied in order to remove Yb^{2+} impurities thanks to the annihilation of the oxygen vacancies by atmospheric oxygen at the ceramic surface. The oxygen incorporation into the grain volume gives rise to the generation of holes ($h^{\bullet}$). In our case, there is an excess of oxygen vacancies in the ceramic grains; the inward diffusion of holes is accompanied by an outward diffusion of the oxygen vacancies $V_O^{\bullet}$, $V_O^{\bullet\bullet}$ which is outlined in reactions Eq. 5, 6.

$$^1/_2\, O_2 + V_O^{\bullet} \rightarrow O_O^* + h^{\bullet} \text{ (5)}$$

$$^1/_2\, O_2 + V_O^{\bullet\bullet} \rightarrow O_O^* + 2h^{\bullet} \text{ (6)}$$

where O_O^* - O^{2-} in YAG lattice.

These holes ($h^{\bullet}$) migrate into the grain body oxidizing Yb^{2+} ions and thus changing the charge state from divalent to trivalent [14].

$$Yb'_Y + h^{\bullet} \rightarrow Yb_Y^* \text{ (5)}$$

It can be assumed that, during air annealing, the amount of Yb^{2+} ions is proportional to the oxygen vacancy annihilation rate and, therefore, to the air annealing duration. It can be hypothesized that a prolongation of the air annealing treatment results in a decrease in Yb^{2+} ions, whereas an increase in the temperature during air annealing speeds up the oxidation rate of Yb^{2+}. These hypotheses led us to investigate the variation of Yb^{2+} concentration during air annealing at three different temperatures, followed by an analysis according to the Jander geometrical model, which allowed to elucidate the Yb^{2+} charge compensation mechanism.

3.1 Structural characterization of the ceramics

The samples were prepared through SSR, a technique in which the powder oxides Y_2O_3-Yb_2O_3-Al_2O_3 are mixed resulting in the formation of the intermediate phases $Y_2Al_4O_9$ and $YAlO_3$ and finally the YAG ceramic [18]. The intermediate phases can be detected in the final sample due to an uncompleted SSR, therefore, it was necessary to prove the phase homogeneity of the samples before conducting the Yb^{2+}

time-dependence experiment. The X-ray diffraction patterns of the prepared ceramics of Yb:YAG show the formation of the pure YAG phase, which matches the Inorganic Crystal Structure Database (ICSD) Card N 170158 (Fig. 1).

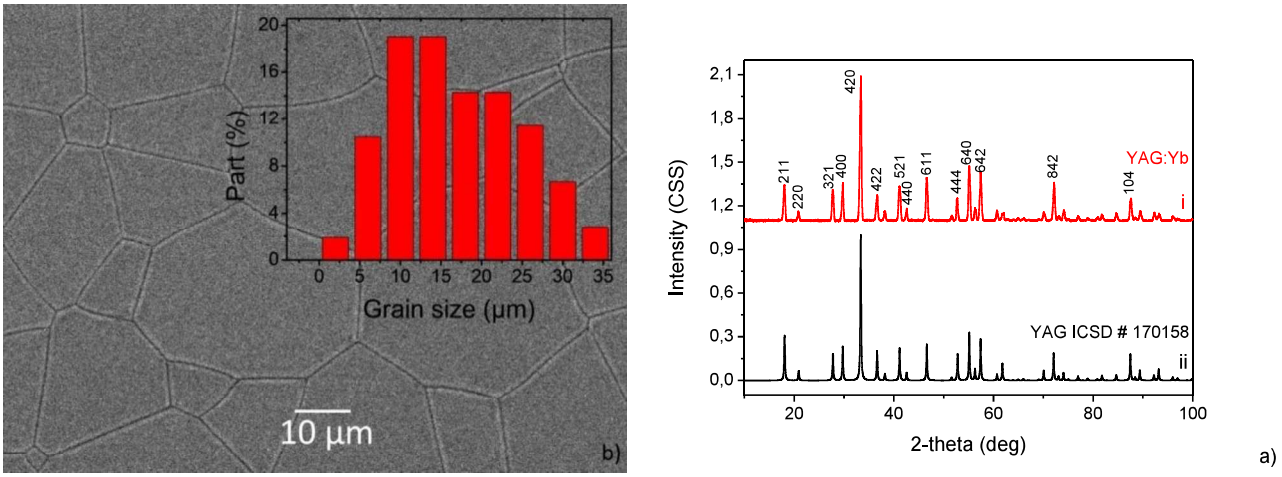

Figure 1: a) X-ray diffraction patterns of Yb:YAG ceramics (i) and ICSD Card N170158 of YAG (ii). b) SEM image of the Yb:YAG ceramics after thermal etching. Inset: Particle size distribution of Yb:YAG ceramic.

Yb atoms replace Y atoms in the YAG crystal lattice because of the minor difference between the ionic radii of Yb^{3+}(0.0985 nm) and Y^{3+}(0.1019 nm) in eightfold coordination [21]. Such a substitution does not appreciably affect the garnet crystal structure. Comparing the diffraction patterns of the Yb:YAG with the undoped YAG, neither the formation of new peaks nor peak shifts were detected. The intensities of the diffraction peaks (Fig. 1) were also identical, meaning that the YAG ceramic grains did not take any preferential orientation.

The Yb:YAG grains morphology was revealed examining the SEM images of the surface after thermal etching. Pores and impurity phase inclusions were not detected on the ceramics' surface (Fig. 1b). The ceramics consist of grains in the range of 3–40 μm with a grain size distribution centred at 12 μm (see inset in Fig. 1b). The results of SEM analysis agree with the XRD patterns indicating that the samples are single phase. Also, it can be noted that the grain size of our samples is in the micron range, while the size of single crystals, which is about two orders of magnitude higher, can be critical to Yb^{2+}

oxidation. Moreover, the oxygen diffusion through grain boundaries is one order of magnitude higher than the diffusion within the grain bodies: a smaller grain size means a greater presence of grain boundaries and, therefore, a higher oxygen diffusion rate, which plays a pivotal role in the Yb^{2+} oxidation process.

3.2 Optical absorption spectra

The Yb^{2+} oxidation process was monitored by measuring the optical absorption spectra during air annealing. The optical absorption spectra of the sintered samples before annealing and the spectra of the fully oxidized samples were recorded for comparison purposes. Fig. 2a shows the absorption spectrum of Yb:YAG ceramic just sintered in a vacuum (3a) and the absorption spectrum of the same ceramic after air annealing at 1300°C for 15 hours (3b). After vacuum sintering, the absorption spectrum of the sample contained the absorption bands of Yb^{3+} and Yb^{2+} ions and colour centres. Narrow peaks were recorded in the vicinity of 1.32 eV, whereas broad absorption bands were located at 1.94, 2.54, 3.24 and 4.48 eV.

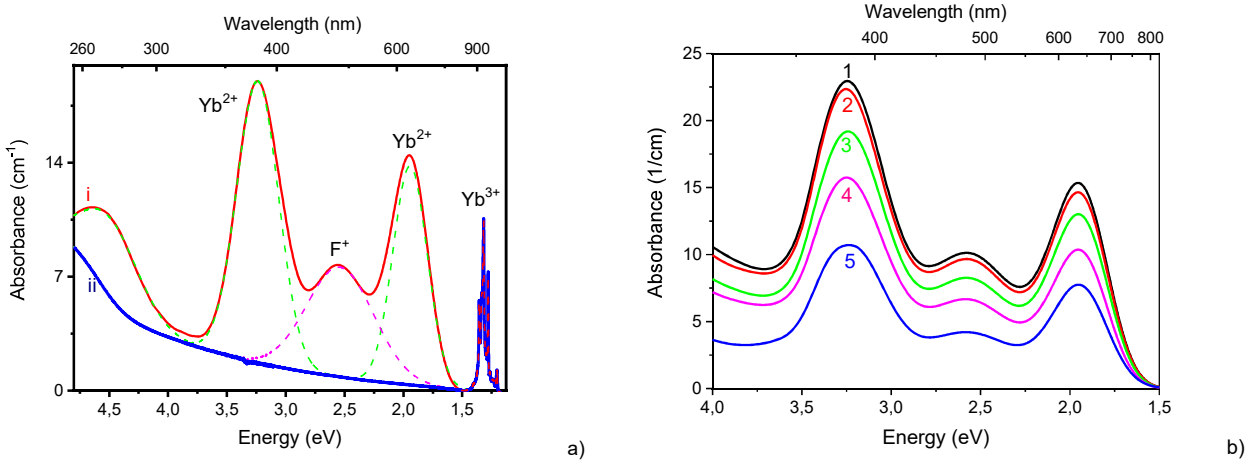

Figure 2: a) Absorption spectra of Yb:YAG ceramic after vacuum sintering at 1750 °C for 10 hours (i), and after air annealing at 1300 °C for 15 hours (ii), the green and magenta absorption bands correspond to Yb^{2+} ions and color centers respectively. b) Difference between the absorption spectra of Yb:YAG ceramic after vacuum sintering and annealing in air at 890°C for 0 min(1), 10 min (2), 40 min (3), 160 min (4), and 760 min

(5).

The absorption peak at 1.32 eV is ascribable to 4f-4f transitions on Yb^{3+}, while the absorption bands at 1.94, 3.24 and 4.48 eV should be assigned to transitions involving the Yb^{2+} ions [14, 15, 22], the broad absorption band at 2.54 eV could originate from unknown colour centres which are probably related to charge compensation defects of the zirconia admixture coming from the milling balls [23]. The absorption band at 1.94 eV, which is located in the yellow part of the visible spectral range, originates from Yb^{2+}–Yb^{3+} intervalence charge-transfer (IVCT) [14]. Thus, comparing the absorption spectra of our sample with that of the YbAG single crystal [14], it is possible to see that, in our ceramic sample, the absorption bands relative to Yb^{2+} ions are all slightly shifted to lower energies; the highest energy band is not shifted, probably due to a lack of sensitivity of our instrument. The YbAG single crystal spectrum has Yb^{2+} bands centred at 2.10, 3.40 and 4.41 eV and an extra one at 3.30 eV which was not detected in the spectra of the ceramic samples. The observed discrepancy in the Yb^{2+} absorption bands might be related to a difference in its formation in ceramics and single crystals.

Yb^{2+} ions and colour centres disappeared after prolonged air annealing at high temperature, thanks to the formation of holes resulting from the oxygen vacancy annihilation by atmospheric oxygen (see Eq 2, 3). Air annealing of the samples at 1300°C for 15 hours resulted in the disappearance of the absorption bands at 1.94, 3.24, 4.48 and 2.54 eV responsible for Yb^{2+} ions and colour centres respectively, whereas the absorption peaks related to Yb^{3+} ions slightly increased in intensity (Fig. 2). Yb^{3+} ions absorption coefficient increased from 10.45±0.01 to 10.57±0.01 cm^{-1} (1.1±0.05%) after air annealing, due to the recharging of Yb^{2+} ions into the trivalent state. This means that a negligibly small amount of Yb^{2+} ions remains after vacuum sintering, and, during air annealing, the oxidation of Yb^{2+} takes place.

3.3 Oxidation kinetics of Yb^{2+}

In the previous section, we showed that air annealing has a significant effect on the Yb^{2+} content, in this section, we are going to report the data relative to the time dependence of the Yb^{2+} amount at three different air annealing temperatures. The experiment was performed by annealing the samples in a special furnace which allows to quickly change the ambient from vacuum to air

and vice-versa. The experimental steps were: (I) heating in a vacuum; (II) annealing in the air; (III) cooling in a vacuum. It is assumed that, under vacuum conditions, the oxidation of Yb^{2+} ions did not take place even at high temperatures. To prove this assumption, the experiments were executed in vacuum at three different temperatures of 860, 890, 920°C, followed by immediate cooling to room temperature without high-temperature air annealing. Negligibly small differences between the absorption spectra of the samples before and after vacuum annealing were observed, indicating that the heating/cooling process did not have any influence on the concentration of Yb^{2+} ions. Therefore, only the duration of the air annealing had an effect on the amount of Yb^{2+} ions.

The influence of the duration of air annealing on the concentration of Yb^{2+} ions was assessed at 860, 890, 920°C by evaluating the collected absorption spectra. Fig. 2b shows the absorption spectra recorded in the range 1.5 – to 4.0 eV of Yb:YAG ceramics annealed at 890°C for different time spans.

The differences in the absorption spectra of the fully reduced and the oxidized samples (Fig 2a) consisted of Yb^{2+} ions and colour centres absorption bands. These spectra were fitted by the FITYK 0.9.8 program [24] to separate the individual peaks into four Gaussian functions (Fig. 2a) [12, 25]. The peaks parameters are presented in Table 1.

Four absorption bands centred at 1.94, 2.54, 3.24, and 4.48 eV were detected. It is possible to note that the highest energy absorption band parameters changed little during the experiments, probably due to the strong overlap with other absorption bands centred in the UV region. The concentration of the Yb^{2+} ions was monitored by measuring the intensity of the peak at 1.94 eV (640 nm) together with the peak at 3.24 eV (380 nm) for comparison. The Smakula-Dexter formula was used (Eq. 8) for estimating the Yb^{2+} ions concentration [26].

$$n = 0.87 \cdot 10^{17} \frac{a_0}{(a_0^2 + 2)^2} \cdot \frac{\delta_{FWHM}}{f} H$$

where n is the concentration of absorbing centres, a_0 is the refractive index of the crystal in the maximum of the absorption band, a_0=1.82, f – oscillator strength, δ_{FWHM} – half-width band absorption coefficient, H – the absorption coefficient at the band maximum. The last two parameters were obtained from the absorption bands centred at 1.94 nm The value for the oscillator power was taken from the literature [14]. Concentrations of Yb^{2+} ions in Yb;YAG

ceramics after annealing at 860, 890 and 920 °C for a different amount of time are reported in Table 2.

Table 1: Characteristics of the absorption bands for the difference between the spectra of fully reduced and fully oxidized Yb:YAG ceramics.

No	V_p, nm	λ_p, eV	δ_{FWHM},eV	H, cm^{-1}
1	638	1.94	0.34	13.4
2	489	2.54	0.67	6.7
3	383	3.24	0.42	17.3
4	277	4.48	0.52	5.2

In our experiment, a prolongation of the air annealing led to a decrease in the amount of Yb^{2+} ions, whereas an increase in temperature sped up the oxidation rate. Only a small fraction of Yb ions existed in the divalent state after vacuum sintering. Because the initial concentration of Yb^{3+} ions in our samples was $0.47 \cdot 10^{22}$ cm^{-3}, we calculated that only 0.25% of Yb ions exist in the divalent state after vacuum sintering, in agreement with the optical absorption measurements, thus validating the suitability of the Smakula-Dexter formula (Eq. 8). Based on these data, we investigated the oxidation kinetics of Yb^{2+} ions in Yb:YAG ceramics, to propose a model for describing the kinetic as well as the charge compensation mechanism of Yb^{2+} ions.

Table 2: Concentrations of Yb^{2+} ions in Yb;YAG ceramics after annealing at 860, 890 and 920 °C for a different amount of time.

920°C		890°C		860°C	
t, min	n, cm^{-3}	t, min	n, cm^{-3}	t, min	n, cm^{-3}
0	$1.13 \cdot 10^{19}$	0	$1.14 \cdot 10^{19}$	0	$1.19 \cdot 10^{19}$
10	$1.16 \cdot 10^{19}$	10	$1.07 \cdot 10^{19}$	10	$1.12 \cdot 10^{19}$
30	$0.90 \cdot 10^{19}$	40	$0.98 \cdot 10^{19}$	50	$1.05 \cdot 10^{19}$
90	$0.81 \cdot 10^{19}$	160	$0.74 \cdot 10^{19}$	230	$0.81 \cdot 10^{19}$
390	$0.61 \cdot 10^{19}$	760	$0.53 \cdot 10^{19}$	1130	$0.62 \cdot 10^{19}$

4. Discussion

In the "Results" section, we presented the data relative to the Yb^{2+} oxidation time dependence at three temperatures, in the following paragraphs, we propose a proper model for describing the Yb^{2+} oxidation. The "Discussion" section is divided into two subsections: in the first one, we describe a model for the Yb^{2+} oxidation according to the Jander geometrical model, while in the second one we present a charge compensation mechanism for Yb^{2+} ions, which is the main purpose of the present work.

4.1 Jander geometrical model

The Yb^{2+} oxidation in the YbAG single crystal [14] as well as in Yb:YAG epitaxial film [15] have been already investigated by some authors. The oxidation kinetics of Yb^{2+} in YbAG crystals was described in the frame of the Wagner model with an approximation of time dependence of Yb^{2+} concentration by the linear-parabolic law [14]. According to the internal oxidation model, under oxidative annealing, the YbAG single crystal can be separated into an oxidized and a reduced area which are clearly detectable. The main difference between these areas is the concentration of Yb^{2+} ions which is approximately zero in the oxidized area and close to the initial value in the reduced area. The oxidation process takes place in three stages: the first one consists in the oxygen adsorption on the surface with the generation of oxidizing defects; the second stage is the diffusion of oxidizing defects across the crystals towards the front of the reduced layer, which contains the Yb^{2+} ions; the oxidation of Yb^{2+} takes place during the third stage, starting from the front of the reduced layer towards the centre of the crystal. Unfortunately, our data on Yb^{2+} oxidation did not fit on the parabolic law, probably because the mathematical proof of this model is based on a flat front of the boundary between oxidized and reduced areas, which can be hardly applied to polycrystalline materials with small grains. We assume that the difference between the oxidation of ceramics and single crystals arises from particularities concerning inter-grain diffusion of oxygen and grain dimensions [27, 28, 29]. The grain boundary oxygen diffusion in the YAG is several orders of magnitude greater than the volume diffusion [30, 31]. Therefore, oxygen can quickly cover the grains and the oxidation takes place as annealing of individual crystals (grains) in an oxygen-rich ambient (oxygen on grain boundary), with a spherical (and not flat) front between the oxidized and the reduced layers.

The Yb^{2+} oxidation process in Yb:YAG ceramics, investigated in the present work, has been treated

under the Jander geometrical model [32]. This model was initially developed to determine the kinetics of the solid-state reaction between two particles that form a core-shell structure which yields to the formation of a product layer between the initial particles. In most cases, the diffusional mass transfer through the product layer and the chemical interactions play a major role in the kinetics of such reactions. The diffusion obeys to the parabolic law as it does in the Wagner model, but the difference between the two models consists in the shape of the reaction front: in the Jander model, it is spherical whereas in the Wagner model it is flat.

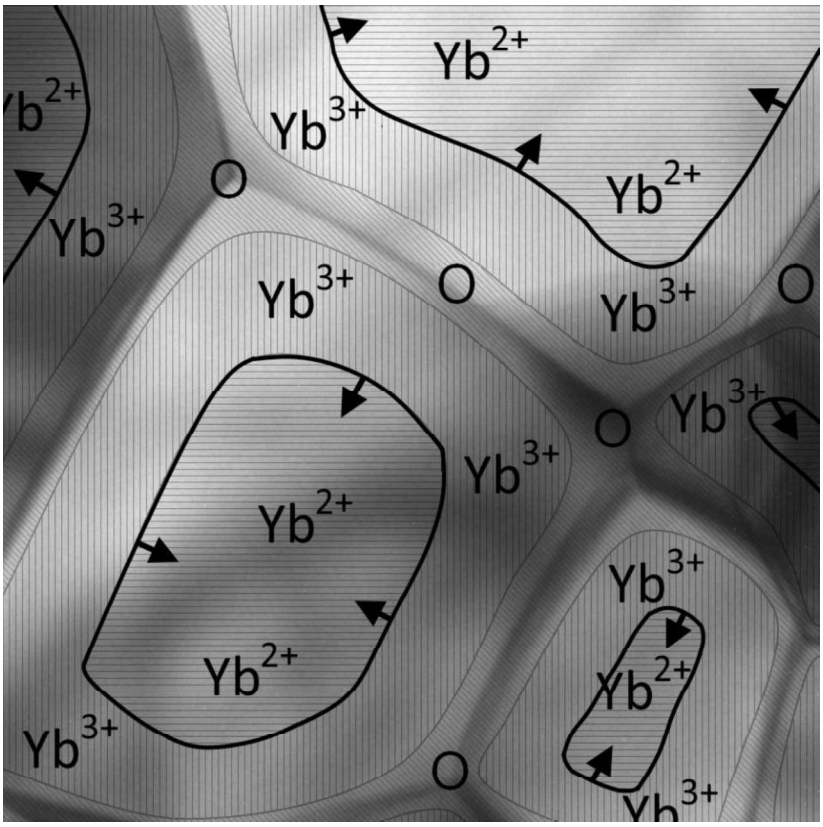

Figure 3: Schematic view of Yb:YAG ceramic layer structure during air annealing, where O, Yb^{2+} and Yb^{3+} denote core, shell and oxidized layer respectively: O - oxygen-rich layer at grain boundary, Yb^{2+} - reduced layer where the concentration of Yb^{2+} was constant and corresponds to the initial value of Yb^{2+} ions and Yb^{3+} - oxidized layer without Yb^{2+} ions. The arrow indicates the direction of the front.

The Jander model can be successfully applied to describe Yb^{2+} oxidation in the Yb:YAG

ceramics where the oxygen-rich layer at the grain boundary represents the "core", the reduced layer represents the "shell" and the oxidized layer represents the "product layer" (Fig. 3). The interaction of oxygen from the grain boundary ("core") with Yb^{2+} in the reduced layer ("shell") leads to the Yb^{2+} to Yb^{3+} ion transformation resulting in the formation of an oxidized layer without Yb^{2+} ions ("product layer").

In the Jander model, the concentration of the chemical species is constant within the layer, only the amount of substance changes, so the rate of the reaction depends on the value *α,* called degree of transformation (see Eq 9).

$$a = (V_0 - V_\tau)/V_0 \text{ (9)}$$

where V_0 is the initial amount of the reduced species, V_τ is the amount of the reduced species at $\tau = 0$. In the case of Yb^{2+}, the oxidation process can be written as:

$$a = (c_0 - c_\tau)/c_0 \text{ (10)}$$

where c_0 is initial concentration of Yb^{2+}, c_τ is the concentration of Yb^{2+} at time *τ,* calculated from the absorption spectra. The Jander model considers two types of equations: one for describing diffusion-limited reactions (see Eq. 11) and another one for reactions limited by chemical processes, which are described by the equations for compressible spheres – kinetic mode (see Eq. 12).

$$\left[1 - (1-a)^{1/3}\right]^2 = \frac{2Dk}{r_0^2}\tau = K_{Y1}\tau \text{ (11)}$$

$$\left[1 - (1-a)^{1/3}\right] = \frac{K_{Y2}}{r_0}\tau \text{ (12)}$$

where D is the diffusion coefficient, r_0 is the radius of the core particle at the initial experimental time (τ), k is the specific coefficient and K_{Y1} and $K_{Y2}$is the Jander constant for diffusion and kinetic modes, respectively. Eq. 11 and 12 were used to calculate the Jander constants for the oxidation process in our Yb:YAG ceramics for reactions taking place in the diffusion (Fig. 4a, curve ii) and kinetic (Fig. 4a, curve i) modes respectively.

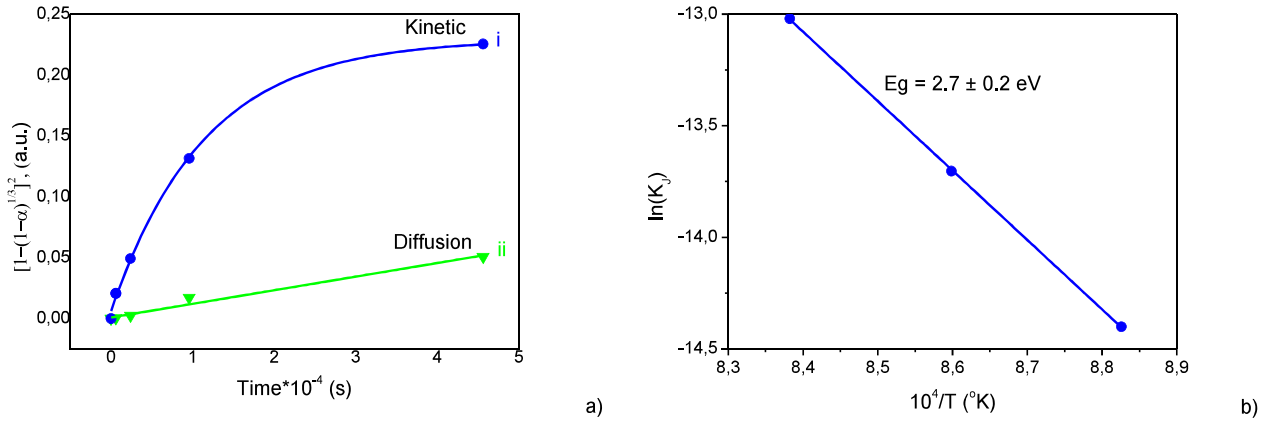

Figure 4: a) Time dependence of Jander constant for kinetic mode (i) and for diffusion mode (ii) under oxidative annealing at 890°C. b) Arrhenius plot of oxidation of Yb^{2+} ions in Yb:YAG ceramics

The linear dependence of the Jander constant on time shows that the variation of the valence state of Yb^{2+} ion in Yb:YAG ceramic is a diffusion-limited process, probably due to the migration of oxygen vacancies as well as oxygen in the YAG lattice. The Jander constants K_Y was determined from the slope of the curve describing the time dependence of Yb^{2+} concentration according to Eq. 11 at each of the three temperatures of 920, 890, 860 °C and the Arrhenius plot was constructed (Fig. 4b).

4.2 Proposed model for Yb^{2+} oxidation in Yb:YAG ceramics

Beforehand, the valence change between the Yb ions in YAG was described in the frame of the Intervalence Charge Transfer model (IVCT, electronic transfer between two metal sites differing only in oxidation state). The term IVCT is used sometimes for electron transfer processes not involving metals, as in our case, where an electron transfer from Yb^{2+} ions to oxygen takes place. In the frame of the IVCT model, Yb^{2+} and Yb^{3+} will not refer to the single Yb ions, but to the defect center they create in the solid [33]. The interactions between donor and acceptor can be described by electronic coupling between the two ionic configurations. For example, Fig. 5 shows

the IVCT configuration coordinate diagram of a Yb^{2+}/Yb^{3+} mixed valence pair in the YAG [33, 34]. The IVCT model mainly focused on the electron transfer between mixed valence ions pairs, while, in our case, the electron transfer between Yb^{2+} ions and oxygen (which replaces the oxygen vacancy), takes place. According to the IVCT model, using different force constants for Yb^{2+} and Yb^{3+} leads to different electron transfer reaction coordinates. Therefore, it is possible that a difference between Yb^{2+} to Yb^{3+} oxidations and Yb^{3+} to Yb^{2+} reduction can occur. This assumption was confirmed by Kreye and Becker, who clearly stated that the activation energy for Yb^{2+} to Yb^{3+} oxidations is lower [14]. In this paper, the Yb^{2+} to Yb^{3+} oxidations process was investigated, without discussing the reverse reaction.

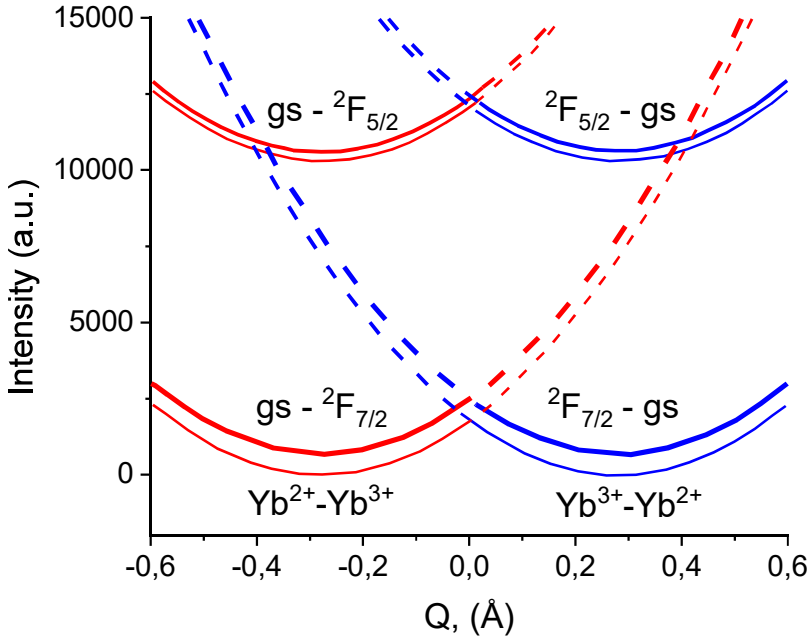

Figure 5: IVCT configuration coordinate diagram of Yb^{2+}/Yb^{3+} mixed valence pair in YAG [33].

The activation energy (E_G) for Yb^{2+} oxidation was determined from the Arrhenius plot to be E_a = 2.7±0.2 eV. This value is the same for that obtaining for Cr^{3+} to Cr^{4+} ion valence transformations in Cr,Ca:YAG ceramic [35]. The E_G of Yb^{2+} oxidation in the Yb:YAG ceramics was higher than the

activation energy for single crystals (1.43±0.12 eV. [14]). It should be noted the presence of grain boundaries neither affects the activation energy nor the presence of colour centres. Typically, grain boundaries play a role in this kind of diffusion-limited reaction paths and the oxidation of Yb:YAG ceramics is equivalent to annealing the small crystals (grains) in an oxygen-rich atmosphere. Also, the effect of F^{+} centres at 2.59 eV on the oxidation kinetics should be considered. These centres correspond to Zr^{4+} charge compensation defects and do not take part in the oxidation of Yb^{2+}, giving rise to parallel processes. Therefore, the difference between the E_G for Yb^{2+} oxidation in single crystals and ceramics derives from the difference in Yb^{2+} charge compensation mechanism and/or impurities composition.

We suppose that there is a difference in the charge compensation mechanism between single crystals and ceramics. For YbAG single crystals, M. Kreye and K. D. Becker concluded that Yb^{2+} oxidation is limited by the migration of anion vacancies [14]. Regarding Yb:YAG ceramics, we obtained a value for Yb^{2+} oxidation E_G in very good agreement with the oxygen diffusion activation energy calculated through molecular dynamics simulations of the YAG lattice (E_a=2.86 eV) [30] and with the energy barrier for oxygen migration in the YAG crystal structure resulting from first principles calculations (2.6 eV) [31]. Consequently, Yb^{2+} oxidation in the Yb:YAG ceramics takes place thanks to the oxygen diffusion through the grain volume, dissimilar to what happens in the YbAG single crystal.

The oxidation of Yb^{2+} ions in YbAG single crystals is limited by diffusion of oxygen vacancies, whereas in Yb:YAG ceramics is limited by oxygen diffusion. It is resulting in different Yb^{2+} charge compensation mechanisms as well as dissimilar Yb^{2+} ions absorption band positions (see "Optical absorption spectra" subsection). M. Kreye and K. D. Becker proposed the next model for Yb^{2+} oxidation in the YbAG single crystal [14]. The starting point of the internal oxidation process is the incorporation of oxygen from the gas phase into the bulk of the solid. The incorporation of oxygen gives rise to the formation of holes and followed transfer to the reaction front. The oxidation of divalent ytterbium ions by holes to Yb^{3+} ions takes place. The inward diffusion of holes can be accompanied by an outward diffusion of oxygen vacancies. The Yb^{2+} oxidation in the YbAG single crystal is limited by outward diffusion of oxygen vacancies. The present paper shown that the oxidation of Yb^{2+} ions in Yb:YAG ceramics take place thorough diffusion of oxygen from grain boundary to the reaction front in contrast to the single crystal.

Two possible Yb^{2+} charge compensation mechanisms are possible in the case of Yb:YAG

ceramics; a previous report concluded that divalent impurities are preferentially located near an oxygen vacancy, forming neutral aggregates in the garnet crystal lattice [20]. During air annealing, oxygen diffuses through the grains destroying these aggregates by relapsing the oxygen vacancy and recharging Yb^{2+} in the trivalent state. Consequently, oxygen vacancies (Eq. 13) and/or oxygen vacancies with antisites (Eq. 14) can be proposed as Yb^{2+} charge compensation mechanism [13].

$$\ll YAG \gg + Yb_Y^* + e' \rightarrow Yb_Y' + {}^1/_2 V_O^{\bullet\bullet} \quad (13)$$

$$\ll YAG \gg + Yb_Y^* + e' \rightarrow Yb_Y' + Y_{Al}^* + {}^1/_2 V_O^{\bullet\bullet} \quad (14)$$

Where $\ll O \gg_{\frac{-}{Y}}$ pure crystal, Y_{Al}^* - Y in the Al position (antisites), Yb_Y^* - Yb^{3+}, Yb_Y' - Yb^{2+}.

Divalent impurities, such as Ca^{2+} or Mg^{2+}, are normally present in the YAG lattice, where they are stabilized by oxygen vacancies [36, 37, 38], this happens as well in the Yb:YAG ceramics, but not in the YbAG single crystals. The formation of Yb^{2+} ions in the Yb:YAG single crystal has been attributed to the presence of tetravalent impurities such as Si^{4+} as charge compensator, [39] alike in the YbAG crystals [14].

Probably, the different Yb^{2+} ions charge compensation mechanism is one of the reasons behind the difference in laser properties of Yb:YAG ceramics and single crystals. Dong *et al.* showed that the laser performance of Yb:YAG single crystal is more sensitive to the Yb concentrations with respect to ceramics, moreover, they find that the laser performance of 20 at.% Yb:YAG ceramic is better than its counterpart single crystal, whereas the performance of 10 at.% Yb:YAG ceramics is worse [9]. We suppose that these discrepancies can be explained by the dissimilar energy transfer in Yb^{3+}-Yb^{2+} pairs caused by different Yb^{2+} charge compensation mechanisms. Yb^{2+} charge compensation mechanism did not arise directly from tetravalent impurities but from the defects they create. Theses defects are determined by Yb:YAG manufacturing technique. Ceramics synthesis occurs in accordance with the corresponding equilibrium phase diagrams of binary or ternary systems, whereas non-stationary processes on the crystallization front play significant role during single crystals growth. The variation of concentrations of the tetravalent impurities don't cause the difference of Yb^{2+} charge compensation mechanisms. However, some limitations are worth noting: our hypotheses were supported only by the difference in activation energies for Yb^{2+} oxidation without carrying out a luminescence study.

Future work should, therefore, include an investigation of the influence of the Yb^{2+} ions on luminescence properties as well as on the energy transfer in Yb^{3+}-Yb^{2+} pairs in Yb:YAG ceramics and single crystals.

5. Conclusions

The garnet ceramics of Yb:YAG were synthesized by vacuum reaction sintering at high temperature, the time-dependence of Yb^{2+} concentration was investigated by air annealing in a special furnace. After vacuum sintering, the absorption spectra of the Yb:YAG ceramics contained four absorption bands which disappeared under air annealing and correspond to the absorption of the Yb^{2+} ions and the F^{+} colour centres, moreover, the absorption bands of Yb^{3+} slightly increased in intensity. A longer air annealing led to a decrease in the Yb^{2+} amount, whereas a higher temperature sped up the oxidation velocity. Only 0.25 at% of Yb ions existed in the divalent state before oxidation. The Yb^{2+} time-dependence was described by the Jander model, allowing to conclude that the Yb^{2+} to Yb^{3+} oxidation process is limited by the diffusion of oxidative agents. The E_G of Yb^{2+} oxidation was $E_a(D)$= 2.7±0.2 eV, which corresponds to the activation energy E_G for volume oxygen diffusion in the YAG lattice. We concluded that the Yb^{2+} oxidation in the Yb:YAG ceramics is limited by oxygen diffusion, meaning that oxygen vacancies and/or oxygen vacancies with antisites compensate for the Yb^{2+} charge, in contrast to the YbAG single crystal where tetravalent impurities are responsible for it.

Acknowledgements

This work was supported by STCU # 5966 project of Targeted Research and Development Initiatives Program, and project # 0113U003231 of The Fundamental Investigation Program. The work was done under the Agreement on scientific cooperation between the National Academy of Sciences of Ukraine and Polish Academy of Sciences. A part of this work has been done based on the collaboration in the frame of International Polish-Ukrainian Laboratory. of Crystalline Optical Materials. M. Chaika received partial financial resources within the confines of financing the PhD scholarship from the project "Multidisciplinary PhD studies - nanotechnology in biomedicine"

(No. POWR.03.02.00-00-IO30/17-00), which is funded by the European Social Funds.

References

[1] Balabanov, S. S., Bykov, Y. V., Egorov, S. V., Eremeev, A. G., Gavrishchuk, E. M., Khazanov, E. A., ... & Zelenogorsky, V. V. (2013). Transparent Yb:$(YLa)_2O_3$ ceramics produced by self-propagating high-temperature synthesis and microwave sintering. Optical Materials, 35(4), 727-730.

[2] Boiko, V., Zeler, J., Markowska, M., Dai, Z., Gerus, A., Bolek, P., ... & Hreniak, D. (2019). Persistent luminescence from Y3Al2Ga3O12 doped with Ce^{3+} and Cr^{3+} after X-ray and blue light irradiation. Journal of Rare Earths, 37(11), 1200-1205.

[3] Vorona, I. O., Yavetskiy, R. P., Doroshenko, A. G., Parkhomenko, S. V., Baumer, V. N., Tolmachev, A. V., ... & Gheorghe, L. (2017). Structural-phase state and lasing of 5–15 at% Yb^{3+}:$Y_3Al_5O_{12}$ optical ceramics. Journal of the European Ceramic Society, 37(13), 4115-4122.

[4] Enrichi, F., Cattaruzza, E., Ferrari, M., Gonella, F., Ottini, R., Riello, P., ... & Zur, L. (2018). Ag-Sensitized Yb^{3+} Emission in Glass-Ceramics. Micromachines, 9(8), 380.

[5] Nizhankovskyi, S. V., Tan'ko, A. V., Savvin, Y. N., Krivonogov, S. I., Budnikov, A. T., & Voloshin, A. V. (2016). Single crystalline YAG: Ce phosphor for powerful solid-state sources of white light. The influence of production conditions on luminescence properties and lighting characteristics. Optics and Spectroscopy, 120(6), 915-921.

[6] Lisitsyn, V., Lisitsyna, L., Tulegenova, A., Ju, Y., Polisadova, E., Lipatov, E., & Vaganov, V. (2019). Nanodefects in YAG: Ce-Based Phosphor Microcrystals. Crystals, 9(9), 476..

[7] Menezes, R. R., Souto, P. M., & Kiminami, R. H. G. A. (2012). Microwave fast sintering of ceramic materials. Sintering of Ceramics–New Emerging Techniques, 1, 3-26.

[8] Maksimov, R. N., Shitov, V. A., Volkov, M. R., Vadimova, O. G. L. V., & Snetkov, I. Y. L. V. (2018). Spectroscopic and laser characteristics of ceramics based on Yb^{3+}-doped Lu_2O_3–Y_2O_3 solid solution. Quantum Electronics, 48(8), 695.

[9] Dong, J., Ueda, K., Yagi, H., Kaminskii, A. A., & Cai, Z. (2008). Comparative study the effect of Yb concentrations on laser characteristics of Yb:YAG ceramics and crystals. Laser Physics Letters, 6(4), 282.

[10] Strek, W., Marciniak, L., Hreniak, D., & Lukowiak, A. (2012). Anti-Stokes bright yellowish emission of NdAlO3 nanocrystals. Journal of Applied Physics, 111(2), 024305.

[11] Brandt, C., Fredrich-Thornton, S. T., Petermann, K., & Huber, G. (2011). Photoconductivity in Yb-doped oxides at high excitation densities. Applied Physics B, 102(4), 765-768.

[12] Chaika, M. A., Dulina, N. A., Doroshenko, A. G., Parkhomenko, S. V., Gayduk, O. V., Tomala, R., ... & Vovk, O. M. (2018). Influence of calcium concentration on formation of tetravalent chromium doped $Y_3Al_5O_{12}$ ceramics. Ceramics International, 44(12), 13513-13519.

[13] Kuklja, M. M. (2000). Defects in yttrium aluminium perovskite and garnet crystals: atomistic study. Journal of Physics: Condensed Matter, 12(13), 2953.

[14] Kreye, M., & Becker, K. D. (2003). An optical in-situ study of the re-oxidation kinetics of mixed valent $Yb_3Al_5O_{12}$. Physical Chemistry Chemical Physics, 5(11), 2283-2290.

[15] Martynyuk, N. V., Ubizskii, S. B., Buryy, O. A., Becker, K. D., & Kreye, M. (2005). Optical in‐situ study of the oxidation and reduction kinetics of Yb‐substituted YAG epitaxial films. physica status solidi (c), 2(1), 330-333.

[16] Chaika, M. A., Vovk, O. M., Doroshenko, A. G., Klochkov, V. K., Mateychenko, P. V., Parkhomenko, S. V., & Fedorov, O. G. (2017). Influence of Ca and Mg doping on the microstructure and optical properties of YAG ceramics. Functional materials, 24(2), 237–243.

[17] Chaika, M. A., Dluzewski, P., Morawiec, K., Szczepanska, A., Jablonska, K., Mancardi, G., ... & Doroshenko, A. G. (2019). The role of Ca^{2+} ions in the formation of high optical quality Cr^{4+},Ca:YAG ceramics. Journal of the European Ceramic Society, 39(11), 3344-3352.

[18] Chaika, M., Paszkowicz, W., Strek, W., Hreniak, D., Tomala, R., Safronova, N., ... & Vovk, O. (2019). Influence of Cr doping on the phase composition of Cr,Ca:YAG ceramics by solid state reaction sintering. Journal of the American Ceramic Society, 102(4), 2104-2115.

[19] Kvapil, J., Kvapil, J., & Perner, B. (1975). O− centre formation in YAG crystals doped with rare earth ions. Kristall und technik, 10(2), 161-165.

[20] Yang, H., Qin, X., Zhang, J., Wang, S., Ma, J., Wang, L., & Zhang, Q. (2011). Fabrication of Nd:YAG transparent ceramics with both TEOS and MgO additives. Journal of alloys and compounds, 509(17), 5274-5279.

[21] Jun, D., Michael, B., & Yanli, M. (2003). Dependence of the Yb^{3+} emission cross section and

lifetime on temperature and concentration in yttrium aluminum garnet [J]. Journal of the Optical Society of America B, 20(9), 1975-1979.

[22] Kushlyk, M., Tsiumra, V., Zhydachevskyy, Y., Haiduchok, V., Syvorotka, I. I., Sugak, D., & Suchocki, A. (2019). Enhancement of the YAG:Ce,Yb down-conversion emission by plasmon resonance in Ag nanoparticles. Journal of Alloys and Compounds, 804, 202-212.

[23] Asatryan, H. R., Kuzanyan, A. S., Petrosyan, A. G., Petrosyan, A. K., & Sharoyan, E. G. (1986). Single crystal growth and investigation of optical and ESR absorption spectra of zirconium- doped YAG. physica status solidi (b), 135(1), 343-352.

[24] Wojdyr, M. (2010). Fityk: a general- purpose peak fitting program. Journal of Applied Crystallography, 43(5- 1), 1126-1128.

[25] Chaika, M. A., Vovk, O. M., Safronova, N. A., Parkhomenko, S. V., Doroshenko, A. G., & Tolmachev, A. V. (2016). Mutual influence of additives of Ca and Si on properties of Cr-doped YAG ceramics. Functional materials. 23(3), 398-403

[26] Dexter, D. L. (1956). Absorption of light by atoms in solids. Physical Review, 101(1), 48.

[27] Permin, D. A., Balabanov, S. S., Novikova, A. V., Snetkov, I. L., Palashov, O. V., Sorokin, A. A., & Ivanov, M. G. (2019). Fabrication of Yb-doped Lu_2O_3-Y_2O_3-La_2O_3 solid solutions transparent ceramics by self-propagating high-temperature synthesis and vacuum sintering. Ceramics International, 45(1), 522-529.

[28] Balabanov, S. S., Gavrishchuk, E. M., Drobotenko, V. V., Palashov, O. V., Rostokina, E. Y., & Yavetskiy, R. P. (2016). A new approach to $Y_3Al_5O_{12}$ transparent ceramics by vacuum sintering of spray-dried xerogels. Ceramics International, 42(1), 961-965.

[29] Balabanov, S. S., Gavrishchuk, E. M., Rostokina, E. Y., Plekhovich, A. D., Kuryakov, V. N., Amarantov, S. V., ... & Yavetskiy, R. P. (2016). Colloid chemical properties of binary sols as precursors for YAG optical ceramics. Ceramics International, 42(15), 17571-17580.

[30] Jun, C., Dong-Quan, C., & Jing-Lin, Z. (2007). Molecular dynamics simulation of thermodynamic properties of YAG. Chinese Physics, 16(9), 2779.

[31] Li, Z., Liu, B., Wang, J., Sun, L., Wang, J., & Zhou, Y. (2012). Mechanism of Intrinsic Point Defects and Oxygen Diffusion in Yttrium Aluminum Garnet: First- Principles Investigation. Journal of the American Ceramic Society, 95(11), 3628-3633.

[32] Jander, W. (1927). Reaktionen im festen Zustande bei höheren Temperaturen. Reaktionsgeschwindigkeiten endotherm verlaufender Umsetzungen. Zeitschrift für anorganische und allgemeine Chemie, 163(1), 1-30.

[33] Barandiarán, Z., Meijerink, A., & Seijo, L. (2015). Configuration coordinate energy level diagrams of intervalence and metal-to-metal charge transfer states of dopant pairs in solids. Physical Chemistry Chemical Physics, 17(30), 19874-19884.

[34] Barandiarán, Z., & Seijo, L. (2014). Intervalence charge transfer luminescence: Interplay between anomalous and 5 d− 4 f emissions in Yb-doped fluorite-type crystals. The Journal of chemical physics, 141(23), 234704.

[35] Chaika, M. A., Tomala, R., Strek, W., Hreniak, D., Dluzewski, P., Morawiec, K., ... & Lesniewska-Matys, K. (2019). Kinetics of Cr^{3+} to Cr^{4+} ion valence transformations and intra-lattice cation exchange of Cr^{4+} in Cr,Ca:YAG ceramics used as laser gain and passive Q-switching media. The Journal of chemical physics, 151(13), 134708.

[36] Doroshenko, A. G., Yavetskiy, R. P., Parkhomenko, S. V., Vorona, I. O., Kryzhanovska, O. S., Mateychenko, P. V., ... & Gheorghe, L. (2019). Effect of the sintering temperature on the microstructure and optical properties of YAG:Cr,Mg ceramics. Optical Materials, 98, 109505.

[37] Bezotosnyi, V. V., Kanaev, A. Y., Kopylov, Y. L., Koromyslov, A. L., Lopukhin, K. V., Tupitsyn, I. M., & Cheshev, E. A. (2020). Influence of CaO/MgO ratio on Cr^{3+} to Cr^{4+} conversion efficiency in YAG:Cr^{4+} ceramic saturable absorbers. Optical Materials, 100, 109671.

[38] Hua, T., Zeng, Q., Qi, J., Cheng, G., Chen, X., Huang, Z., Lu, T. (2018). Effect of calcium oxide doping on the microstructure and optical properties of YAG transparent ceramics. Materials Research Express, 6(3), 036203.

[39] Henke, M., Persson, J., & Kück, S. (2000). Preparation and spectroscopy of Yb^{2+}-doped $Y_3Al_5O_{12}$, $YAlO_3$, and $LiBaF_3$. Journal of luminescence, 87, 1049-1051.